Spatiotemporal Landslide Activity Derived from Tree-rings: The Tieliku Mingsui Landslide, Northern Taiwan

Jeff Keck[1]*   Cheng-Yang Hsiao[1]   Bor-Shiun Lin[1]   Ming-Hsun Chan[2]   William Wright[3]

ABSTRACT   Spatiotemporal landslide activity records are reconstructed for the Tieliku Mingsui landslide. Periods and the extent of scar activity at the foot of the landslide body are estimated from satellite and aerial photo records. The location of landslide features at the densely forested head of the landslide body are surveyed in the field using a VBS-RTK survey and periods of activity are inferred from growth disturbances recorded in 14 conifer and broadleaf trees growing adjacent to the features. Together, image and growth disturbance records produce a detailed spatiotemporal landslide activity record that spans 34 years and includes 8 years of activity. A comparison of landslide activity records with rainfall data collected near the landslide reveals that years of landslide activity coincide with years of high summer season and event accumulated rainfall.

Key Words : Dendrogeomorphology, landslide activity, VBS-RTK survey, rainfall threshold.

I. Introduction

High intensity typhoon rain events annually lash the steep, tectonically active mountains of Taiwan (Chen and Chen, 2003; Wang et al., 2003). Settlements and roads, which have been carved into even the most remote and steepest headwaters, are frequently exposed to rainfall caused landslide hazards. Recent examples include rain caused landslides that have instantaneously buried entire villages (Tsou et al., 2011) and landslides which caused rapid bed aggradation and the inundation of near river infrastructure(Capart et al., 2010). In such a volatile mountain setting, identifying landslide hazards is critical to successful disaster mitigation efforts.

Landscape scale landslide hazard mapping has been well described in the literature and includes physical model based methods(Montogomery and Dietrich, 1994; Borga et al., 1998) and statistical based methods(Chang et al., 1999; Pistocchi et al., 2001). The spatial extent and failure type of individual landslides can be further clarified via field investigation and survey of tension cracks, secondary scarps, and scars around the landslide(Cruden and Varnes, 1996; Cornforth, 2005). Landslide activity can be inferred from multi-temporal remote sensing measurements or repeated field surveys(Cruden and Varnes, 1996; Montgomery et al., 2000; Tcai et al., 2011). Assuming landslides features formed on a slope covered by trees, years of landslide activity can also be estimated from a dendrogeomorphic survey on the trees growing near landslide features. This method was successfully used to date rock slides(Schroder, 1978), landslides(Braam et al., 1987; Fantucci and Sorriso-Valvo, 1999; Carrara and O'neill, 2003; Lopez et al., 2011; Lopez et al., 2012) and debris flows(Bollschweiler et al., 2007). Once periods of

landslide activity are known, and if coincident hourly rainfall records are available, specific rainfall characteristics associated with landslide activity can be identified(Larsen and Simon, 1993; Montgomery et al.; 2000; Gabet et al., 2004; Tcai et al.,2011; Lopez et al., 2011).

In this study, remote sensing, field survey and dendrogeomorphic methods are used to identify the location and years of activity of a medium sized, deep seated landslide in northern Taiwan. Aerial photo and satellite images are used to estimate periods of landslide activity based on scar evolution at the foot of the landslide. Landslide activity at the head of the landslide is estimated from a dendrogeomorphic survey conducted on a mixed tree species sample group located on the head of the landslide. Specifics regarding dendrogeomorphic methods, including sampling, crossdating and growth disturbance identification methods are detailed. The resulting spatiotemporal landslide activity record spans 34 years and includes 8 landslide events. Using hourly rainfall data from a nearby rainfall station, specific rainfall characteristics of the storm events that occurred during years of landsliding are identified.

II. Study Area

The landslide is located 40 km upstream of the Shihmen reservoir, on the west face of a low elevation(700m to 900m) ridge in the northern mountains of Taiwan (Fig. 1). The ridge is blanketed by bamboo plantations and 30 to 60 year old mixed conifer and broadleaf forests. Regolith is comprised of a 1 meter deep rocky soil layer covering a thick, highly fractured argillite and sandy shale stone bedrock(Taiwan CGS, 2012). The landslide extends from the ridgeline to the Taiyao No. 2 stream at the base

〔1〕財團法人中興工程顧問社防災科技研究中心
  Disaster Prevention Technology Research Center, Sinotech Engineering Consultants, Inc., Taipei, Taiwan.
〔2〕國立嘉義大學森林暨自然資源學系
  Department & Graduate Institute of Forestry and Natural Resources, National Chiayi University, Chiayi, Taiwan.
〔3〕土桑市亞利桑納大學樹木年輪研究實驗室
  Laboratory of Tree-Ring Research, University of Arizona, Tucson, Arizona, USA.
* Corresponding Author. E-mail : keckje@gmail.com

of the slope and has a plan area of roughly 1.5 ha and an estimated width of 125 meters. The exact depth of the slide is unknown, however, in this study, the landslide is described as deep seated because failure appears to be occurring within bedrock rather than the overlaying soil(Roering et. al., 2005; Migon et al., 2010) and medium sized based on size classification described in Cornforth (2005).

The topography of the landslide is overall neither strongly converging or diverging and includes a small ridge like bulge flanked by two poorly defined swales. A road that provides access to many of the villages on the east side of the Yufeng river cuts across the base of the landslide. Also, during the last 15 years, as a result of natural fluvial processes and the installation of a series of check dams, the Taiyao No. 2 stream appears to have actively widened and deposited or eroded new debris at the base of the slope (Fig. 3).

Though not entirely symmetric, based on topography and the configuration of landslide features, the landslide resembles an idealized rotational landslide (IAEG Commission on Landslides, 1990). The main body of the landslide still remains perched on the hillslope. A landslide scar marks the foot of the landslide, where frequent shallow landsliding has depleted the zone of accumulation. A 2 to 5 meter tall main scarp and zone of step like tension cracks surrounds the top of the landslide body, near the ridgeline.

The bedrock exposed along the main scarp is degraded and fractured such that no clear bedrock dip direction is measureable. However, measurements made along a road cut bank 150 meters southwest of the foot of the landslide indicate that the bedding dips 20 to 40 degrees to the east, suggesting that the slide is not translationally sliding along any specific bedding plane. It should be noted that the main scarp at the head of the landslide continues in a northeast direction beyond the zone of fresh tension cracks, indicating that the landslide may be a portion of a much larger and older slide.

III. Methodology

1. Remote sensing observations

Remote sensing observations were used to identify landslide extent and include a 2010 air LiDAR DTM data set and a series of ortho-corrected aerial photo and satellite images recorded between 1985 and 2010(Fig 3). Periods of scar activity and the area of the scar were obtained from the ortho-corrected images. The scarp surrounding the top of the landslide body is visible in aerial photos as a northeast-southwest oriented linear gap in the forest canopy(Fig 2 A) and a similarly oriented zone of high slope is also clear in 2010 Air LiDAR topographic data (Fig 2 B).

2. Field survey

A VBS-RTK system was used to survey the location of landslide features and trees located on the head of the landslide(Fig. 4 A). The VBS-RTK survey system was selected to minimize horizontal error associated with typical handheld GPS receivers and ensure that the relative location of trees and land slide features were correctly mapped. During the survey, the estimated horizontal error recorded by the VBS-RTK system ranged from 0.2 m to 3.0 m. Features were surveyed by traversing and recording locations at bends or regular intervals along the feature.
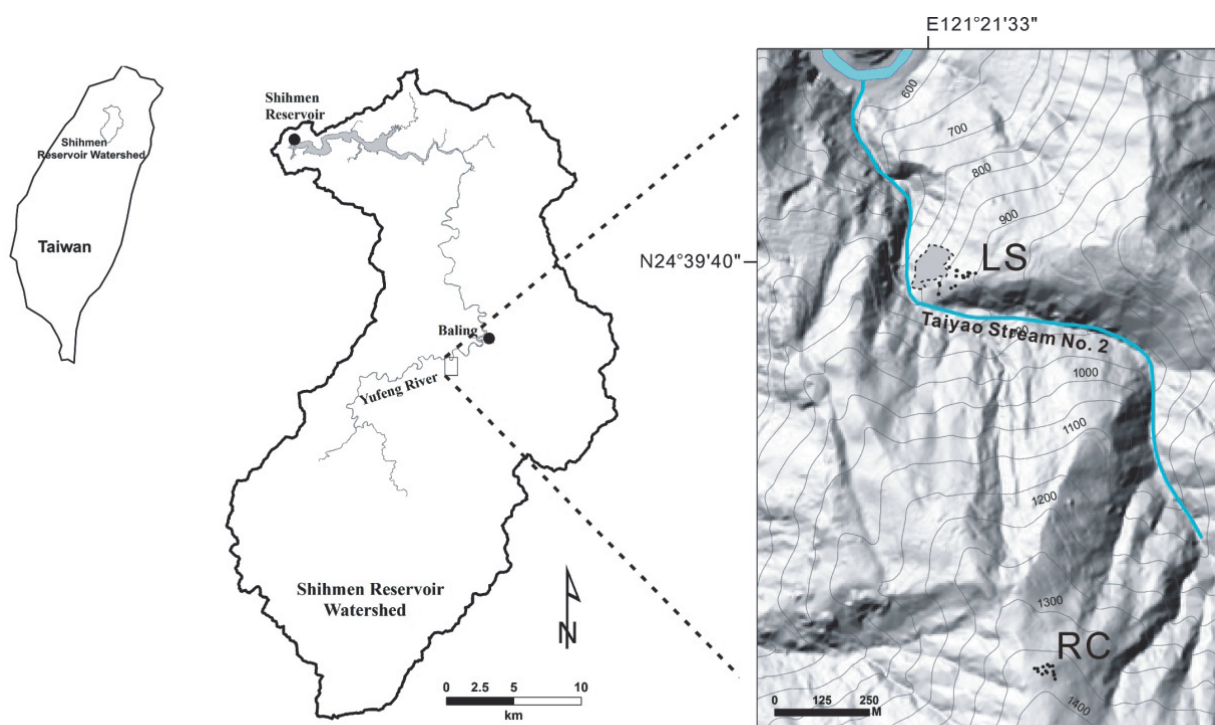
Fig.1 The landslide and adjacent trees (LS) and the reference trees(RC) are located upstream of the Shihmen reservoir on the east side of the Yufeng river

3. Dendrogeomorphic investigation

Dendrogeomorphic investigations, such as the one implemented in this study, utilize the annual rings of trees to date past geomorphic processes (Alestalo, 1971). Trees growing near a landslide that also exhibit signs of physical disturbance, such as tree lean, a disrupted root system, accumulation of debris at the base of the tree or scars in the bark of the tree may have annual rings that formed while being affected by a landslide-caused growth disturbance (Stoffel et al., 2010). Growth disturbances detectable by analyzing the width of the annual rings can be separated into 4 types including: death, suppression, release and the formation of reaction wood(Schroder, 1978; Stoffel et al., 2010).

For this study, a total of 17 trees were sampled from the head of the landslide. The landslide sample group included four tree species: Alnus formosana, Liquidambar formosana, Cunninghamia konishii and Cinnamomum camphora. Only trees that were growing in areas marked by landslide features such as tension cracks, the landslide scarp and fresh colluvium deposits were selected for sampling. Many of the sampled trees were leaning. Often, leaning trees will try to regain a vertical orientation by bending(Speer, 2010). From each tree, four radius cores were extracted orthogonally at the location of most severe bending or at breast height if no obvious bending existed(Fig. 4 B). A reaction wood and suppressed wood core were extracted in the direction of the tree lean and two normal wood cores were extracted perpendicular to the direction of the tree lean, one from each side of the tree. Cores were extracted so that they included the pith of the tree, however some cores did not include the pith.

For each tree, the tree species, tilt direction and the direction of each core were recorded. Tree species was especially important to note since the side of the tree that reaction wood forms differs for conifer and broadleaf trees: conifer trees form reaction wood in the direction of the lean while broadleaf trees form reaction wood on the side of the tree opposite the direction of the lean(Wang, 1984).

In order to identify and rule out other factors that may affect tree growth such as climate or stand wide disturbances(Fritts, 1976; Cook and Kairiukstis, 1990), growth patterns observed in landslide affected trees were compared to a control or reference chronology. The reference chronology was developed using 15 Cryptomeria japonica trees, aged 35 to 39 years old, growing on a north facing ridge approximately 1 km south of the landslide (Fig. 1) under similar environmental conditions but unaffected by the landslide (Schroder, 1978; Lopez et al., 2012). A sampling orientation perpendicular to the fall line of the slope was chosen for the reference trees, to exclude the potential effects of soil creep caused reaction wood. Age effects on tree growth were accounted for using tree ring standardization techniques (Stokes and Smiley, 1965; Fritts, 1976; Cook and Kairiukstis, 1990; Feng and Chan, 2012; Lopez et al., 2012).

(1) Crossdating

Due to the highly disturbed nature of the landslide trees and differences in growth rates associated with each tree species, only visual and graphical checks were used to crossdate small segments of the ring width series. Reference chronology trees however, were crossdated using visual, graphical and statistical crossdating checks as shown in Fig.5.
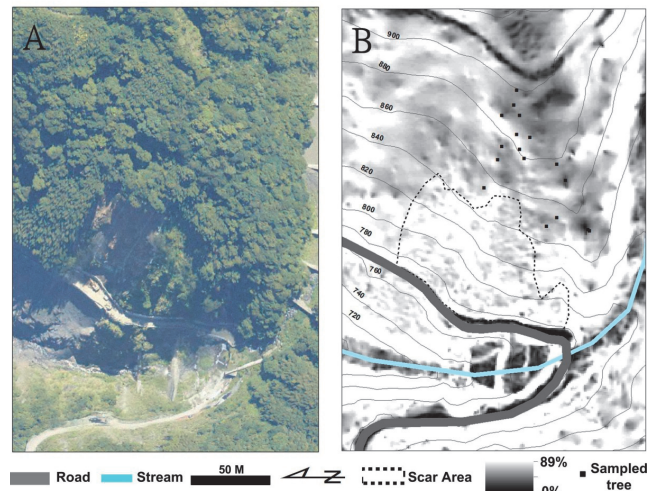
Fig.2 (A) 2008 Aerial photo of the landslide showing scar at foot of slide and canopy gap upslope of scar. (B) 2010 Air LiDAR topography of landslide, shaded according to percent slope. The area of high slope just below the ridge, located in the same area as the canopy gap visible in the aerial photo, is the location of the landslide scarp verified in the field
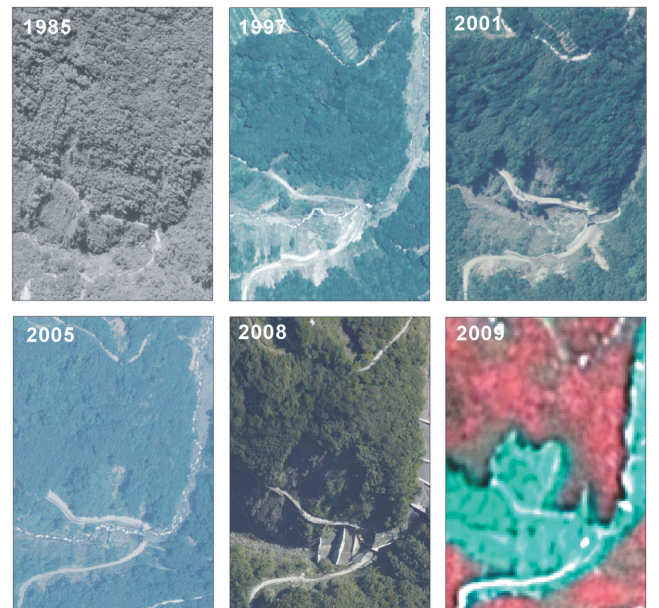
Fig.3 Ortho-corrected aerial photo and satellite images of the hillslope
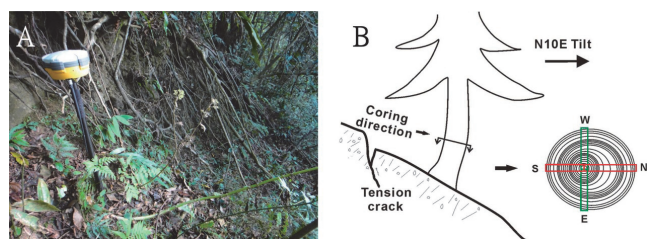
Fig.4 (A) The relative locations of landslide features and trees where confirmed using a VBS-RTK survey. (B) Four radius cores(two diameter cores) were extracted from each tree

Visual examination of each core was the first and perhaps most important step in the crossdating procedure. Before visual crossdating could begin, each core was prepared using standard sample preparation techniques(Speer, 2010). Cores were then visually crossdated by simultaneously examining the cores from the same tree using a 10 to 40X power stereo microscope. Ring characteristics such as year to year variation in ring width, color and structure were used to aid visual crossdating. Once cores from a single tree were successfully visually crossdated, cores from separate trees were also compared and checked for consistencies in ring characteristics.

Before graphical crossdating could be performed, each core was converted to an individual ring width series. Creating the individual ring width series involved scanning the core using a 2400 dpi photo scanner and manually measuring the width of each ring from the image using image analysis scripts written in MATLAB. Once created, the ring width series were plotted and year to year variations in width compared.

Individual width ring width series extracted from the same tree and unaffected by reaction wood often showed similar year to year changes in ring width and were easily matched. Ring width series that included periods of reaction wood or other disturbances were much more variable. Consequently, cross dating of the reaction wood ring width series often relied on matching pointer years, or years of extremely slow or fast growth observable in the ring width series and the reference chronology. Before edits were made to the ring width series, each edit was visually reexamined to confirm the presence or non-presence of a ring or similar ring characteristic such as color or structure.

Fig.6 shows how the northwest(NW) core of a Cunninghamia konishii tree was edited using visual and graphical crossdating techniques. This conifer was found growing along the edge of the main scarp and leaning heavily to the NW. Many years of fast and slow growth observable in the SE, NE and SW ring width series match years of fast and slow growth in the reference chronology(RC). Missing and false rings associated with the formation of reaction wood were numerous in the NW core. However, by using graphical checks paired with visual re-examination of the core, initial visual crossdating errors were corrected. Fig.6 illustrates how two of the cross dating errors were corrected. At location A, three rings were incorrectly interpreted as false rings during initial visual crossdating. By graphically comparing the NW ring width series to the three other individual ring width series and the reference chronology, the false rings were corrected as annual rings. At location B, a small ring originally interpreted as an annual ring in the northwest core was corrected as a false ring, which shifted the whole series behind B forward one year and better matched the other three individual ring width series and the reference chronology.

A final statistical check on the reference chronology tree ring width series was performed using COFECHA. (Holmes, 1983; Grissino-Mayer, 2001). After completing visual and graphical crossdating, each individual tree ring width series was entered into COFECHA to create a single master dating series and evaluate the quality of cross-dating by intercorrelation between each individual tree series and the master dating series. Due to the young age of the trees, series intercorrelation was examined using spline lengths of 10, 15, 20 and 30 years. A maximum value of 0.452 was obtained using a spline length of 20 years.
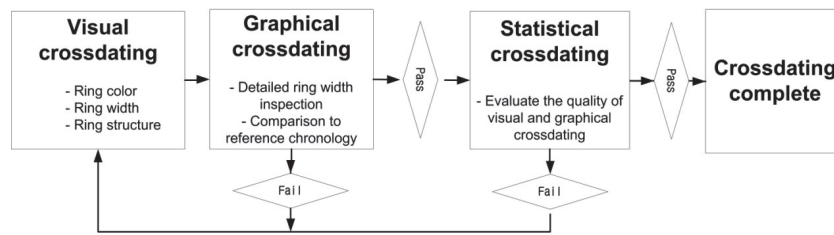
Fig.5 Crossdating work flow is divided into visual, graphical and statistical crossdating. Only visual and graphical checks were used to crossdate the landslide trees
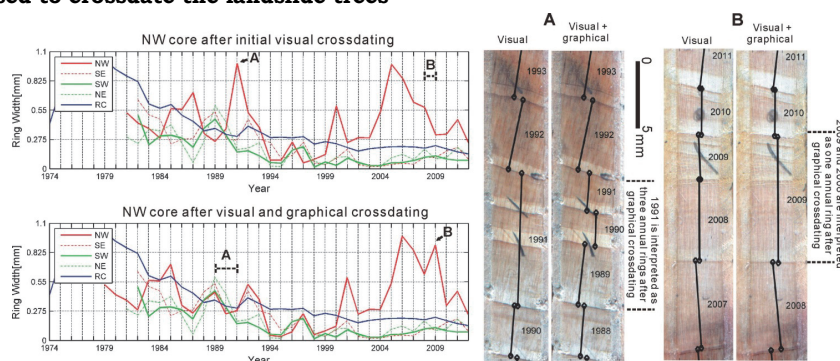
Fig.6 Graphical crossdating and visual reexamination of NW facing reaction wood core of a Cunninghamia konishii. The core was visually reexamined to check that visual characteristics in the wood matched edits at points A and B in the ring series. Black lines drawn on the core images are actual measurement locations before and after being edited

Series intercorrelation standards vary according to tree species and geographic region (Grissno-Mayer, 2001; Speer, 2010). However, values greater than 0.516 are desirable when obtained using a 20 year spline, (Grissno-Mayer, 2001) and any series below 0.516 should be reexamined. After reexamination of the reference tree ring series, two ring series which had a correlation to the master dating series lower than 0.300 were removed from the master dating series, and an intercorrelation of 0.522 was obtained for the remaining 13 trees. The average mean sensitivity of the reference chronology trees was 0.216, which is near the generally accepted value of 0.2 for climate reconstruction(Speer, 2010) and falls between the suggested range of 0.2 and 0.3(Grissino-Mayer, 2001).
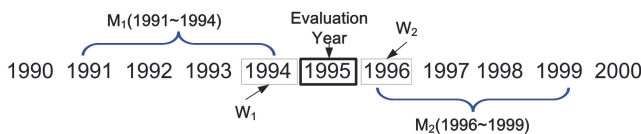
(2) Growth disturbance analysis

Once successfully crossdated, each tree ring width series from the landslide sample was then analyzed for the presence of growth disturbances. A double moving window(Braam et al., 1987) was used to identify three types of growth disturbances: 1) sudden growth release, 2) sudden growth suppression and 3) formation of reaction wood. (Schroder, 1978; Baker et al., 2005; Bollati et al., 2007; Lopez et al., 2012). No dead trees suitable for sampling were found on the landslide.

① Suppression and release

Negative changes in the ring width series were interpreted as suppression events and positive changes were interpreted as releases. Ring width series were analyzed for the presence of sudden growth changes using the following four year average and year to year assessment criteria:

A. Four year average growth change of at least 50% (Baker et al., 2005; Bollati et al., 2007; Wang and Zhao, 2011).
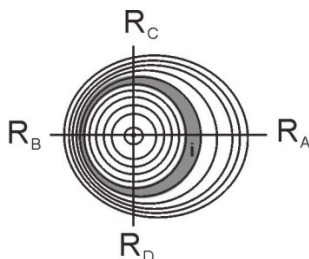
$$\left|\frac{M_1 - M_2}{M_1}\right| \times 100\% > 50\% \tag{1}$$

B. Year to year change of at least 50% (Lopez et al., 2011)

$$\left|\frac{W_1 - W_2}{W_1}\right| \times 100\% > 50\% \tag{2}$$

Where M1, M2 are the four year average width of the rings before and after the year being analyzed and W1 and W2 are the ring widths of the year before and after the year being analyzed (Fig. 7).

Only changes in the ring width series that for the year being analyzed simultaneously met both average and year to year growth change criteria were considered a suppression or release event for that ring width series. The suppression or release event was not considered an event for the tree unless at least 3 ring width series from the tree simultaneously exhibited the same growth disturbance(Baker et al., 2005).

② Presence of reaction wood：

The presence of reaction wood was determined for each year by measuring sudden changes in the eccentricity of the annual rings using an eccentricity measurement modified after Alestalo (1971) and Braam et al. (1987), as defined by equation 3. Using ring widths measured along the same diameter of the tree, the difference in ring width between the reaction wood side of the ring, and that of the opposite side of the ring were determined and divided by the summation of the two ring width measurements:

$$E_{ABi} = \frac{R_{Ai} - R_{Bi}}{R_{Ai} + R_{Bi}} \tag{3}$$

Where RAi is the width of ring i measured in the reaction wood side of the tree, or radius RA and RBi is the width of the ring i measured in the core opposite the reaction wood side of the tree, or radius RB. (Fig.8) Using both sets of radius cores, eccentricity EABi and EDCi where determined.

Changes in eccentricity were again analyzed using a double moving window. For this study, only significant changes in eccentricity that resulted in an increase in the absolute value of eccentricity were considered an indication of reaction wood growth. Significance was assessed using a two tailed T test(Bramm et al., 1987). Assuming equal sample variance and using the null hypothesis that the average eccentricity of the first moving window was equal to that of the second, years in which the t value exceeded the critical value for a 99% confidence level were identified as years of significant change in eccentricity. For this study, only one

Fig.7 Four year average and year to year comparison method used on each ring width series

Fig.8 Illustration of tree cross-section that has formed reaction wood along radius RA. The eccentricity measurement defined by equation 3 compares the width of ring i measured along the radius RA to the width measured along radius RB

set of radius cores needed to exhibit significant eccentric growth for the eccentric growth to be recorded and considered a reaction wood formation event for the tree.

　　For each tree, growth disturbance analyses were automatically performed and summarized as a growth disturbance history card so that results could be visually checked. A growth disturbance history card for the Cunninghamia konishi crossdated in Fig.6 is shown in Fig. 9. Years that suppression, release and formation of reaction wood events occur are indicated using a red, green or yellow bar respectfully and tabulated at the base of the card. The actual appearance of the suppression, release and reaction wood formation events visible in cores are shown in Fig. 10.

(3)　Interpretation of Landslide events

　　Typical dendrogeomorphic studies use a growth disturbance index value to interpret landslide activity from the trees exhibiting growth disturbance(Schroder et al., 1978, Lopez et al., 2011). Due to the small sample size employed in this study, and the structure of the landslide, an alternate approach based on methodology used in Bollschweiler et al. (2007) was applied. In that study, rather than an index val-

ue, the spatial location of growth disturbance events relative to the location of debris flow channels were used to identify when specific channels were active. In this study, we use the location of growth disturbances to identify when specific landslide features were active. Our assumption is that the landslide body moved only several meters during sliding and that the movement may have been largely isolated to a specific area or sliding surface of the landslide.

　　Landslide features are considered to have been active if at least 2 trees growing near the same landslide feature exhibited growth disturbances during the same year. Any year that a feature is active is considered a landslide event. During years of continuous activity along the same feature, only the first year of activity is considered to coincide with the growth disturbance triggering landslide event(Bramm et al., 1987), however because the formation of reaction wood in some trees may be delayed several years (Carrara and O'Neill, 2003), the spatial location of all reaction wood formation events for the year of and the year following the landslide event were used to identify the spatial extent of activity along the feature.
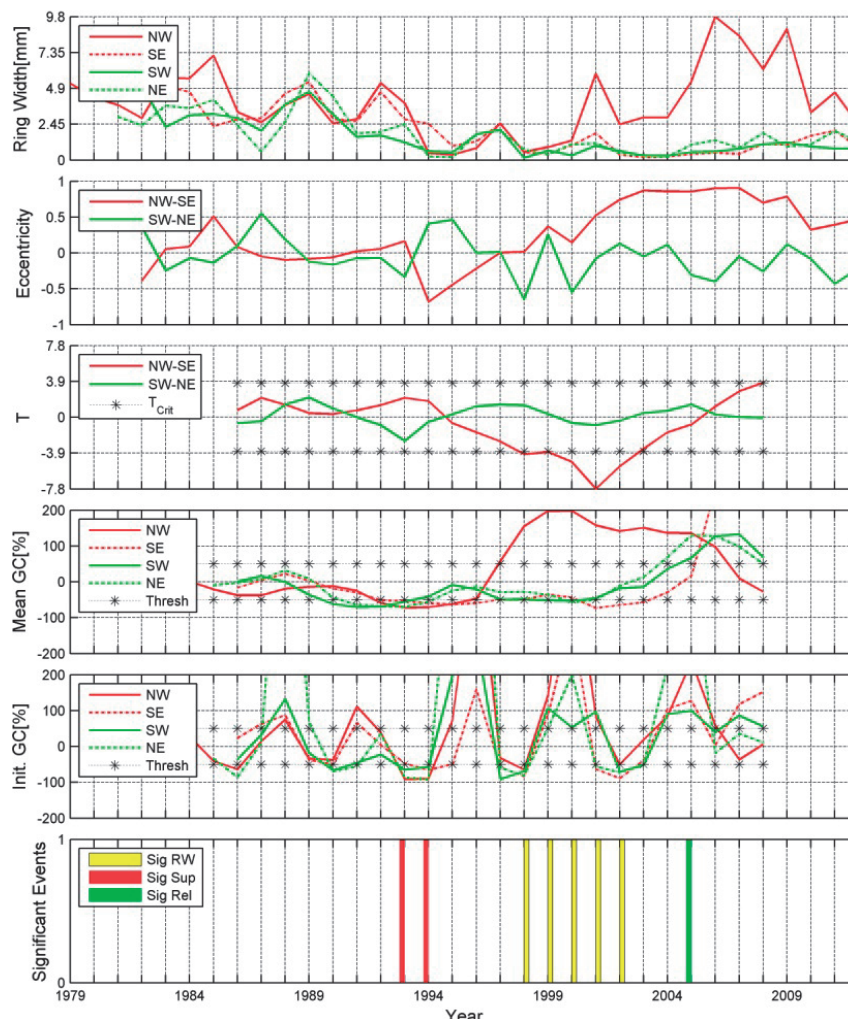
Fig.9　Growth disturbance history card for Cunninghamia konishii crossdated in Fig 6. Suppression and release events were recorded in at least three cores for years 1994 and 2005 respectively. The NW core formed reaction wood between 1998 and 2002

IV. Results

1. Spatiotemporal landslide activity

Of the 17 trees sampled at the landslide, 3 trees, two Cinnamomum camphora and one Liquidambar formosana had rings that were so poorly defined that visual crossdating within the tree was impossible. Of the 14 successfully crossdated trees, except for three trees that began growing before or during the 1950's, all other trees began growing before or during the 1970's. The average age of the 14 cross dated trees at the location and time of sampling was 42.5±9 years.

Using the survey, remote sensing and dendrogeomorphic analysis methods presented in this study, the location and date of 8 landslide events were identified and are shown in Fig.11. For each year of activity, the location of scar activity at the foot of the landslide and/or growth disturbance causing landslide activity at the head of the landslide is shown. A histogram showing the year and area of scar enlargement and year of growth disturbance events is shown in Fig.12. In both figures, growth disturbances are colored according to disturbance type with reaction wood formation, suppression and release events colored yellow, red and green respectively. Landslide activity at the Tilieku Mingsui landslide is described as follows:

Activity began in 1976, when trees growing next to a present day tension crack exhibited suppression and reaction wood formation events. Years later in 1985, a narrow landslide scar formed along the north edge of the landslide body and two reaction wood forming growth disturbance events occurred directly upslope of the scar near a common tension crack. Following landsliding and subsequent growth disturbances in 1990 were again along the lower tension crack that moved in 1976. In 1993, a suppression event and a reaction wood formation event were recorded. However, because the two trees did not border the same landslide feature, they were not considered a landslide event.

In 1998, trees located along what today appears as the main scarp simultaneously exhibited reaction wood formation events, perhaps indicating the year that movement first occurred along the main scarp during the life of the sampled trees. In 2003 and 2004, several release events were recorded, however, because the events were not located near a common landslide feature, they were not considered landslide events. In years 2005 and 2008, two more landslide events occurred. Both events were located along the main scarp and also coincide with years of scar enlargement. Growth disturbances in 2005 included several release events and one reaction wood formation event near the main scarp while 2008 included reaction wood formation and suppres
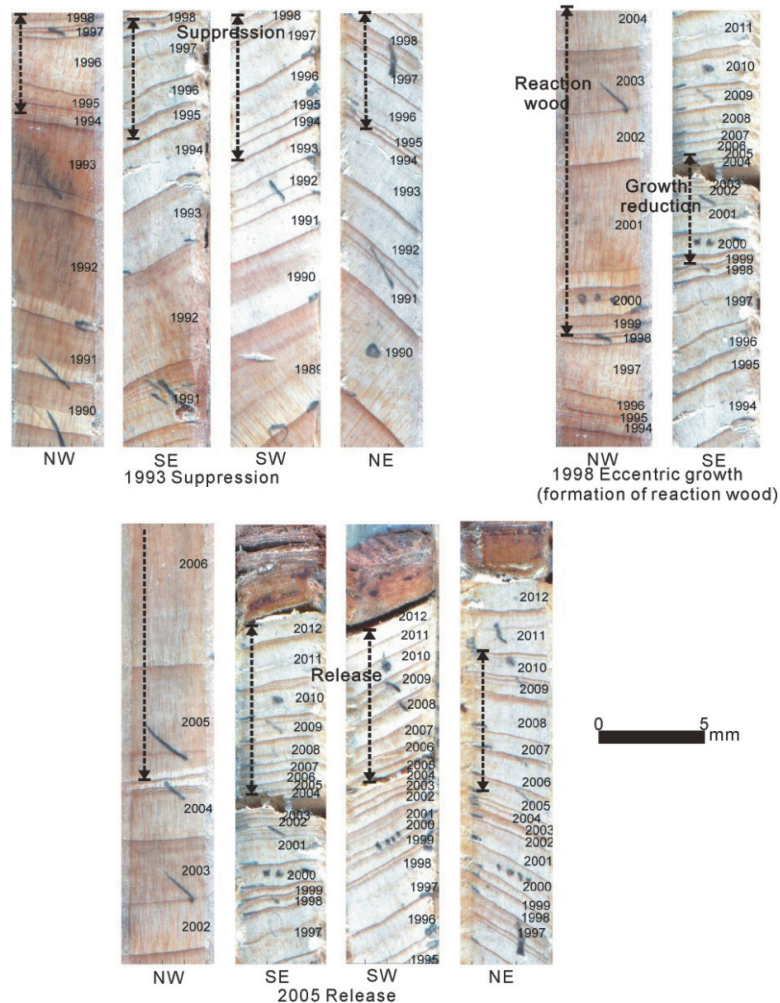
Fig.10   Suppression, release and reaction wood formation events visible in cores extracted from Cunninghamia konishi crossdated in Fig 6

sion events near the main scarp. In 2009, the scar continued to enlarge at two locations along the upper edge of the scar.

During the landslide process, the most frequent growth disturbance type was the formation of reaction wood. The highest number of growth disturbances within a single year occurred in 2005. The primary growth disturbance in 2005 was sudden release. Since the reference chronology does not exhibit sudden growth in 2005 and the release events recorded at the landslide were tightly grouped near the main scarp, the release disturbance may have been caused by a local, possibly landslide caused disturbance.

2. Rainfall and landslide records

Hourly rainfall data collected from a rainfall station located 1 kilometer north of the landslide was used to compare annual and event rainfall conditions to the landslide activity record for each year between 1974 and 2011. This period was selected because the majority of the sampled trees were already well established by 1974 and the last year of available remote sensing data is 2011. Rainfall events were defined using method 5 described in Jan et al. (2003), where a storm event begins the first hour that 1 hour accumulated rainfall exceeds 4 mm and ends the final hour of the first continuous 6 hour period that maximum 1 hour accumulated rainfall is less than 4 mm.
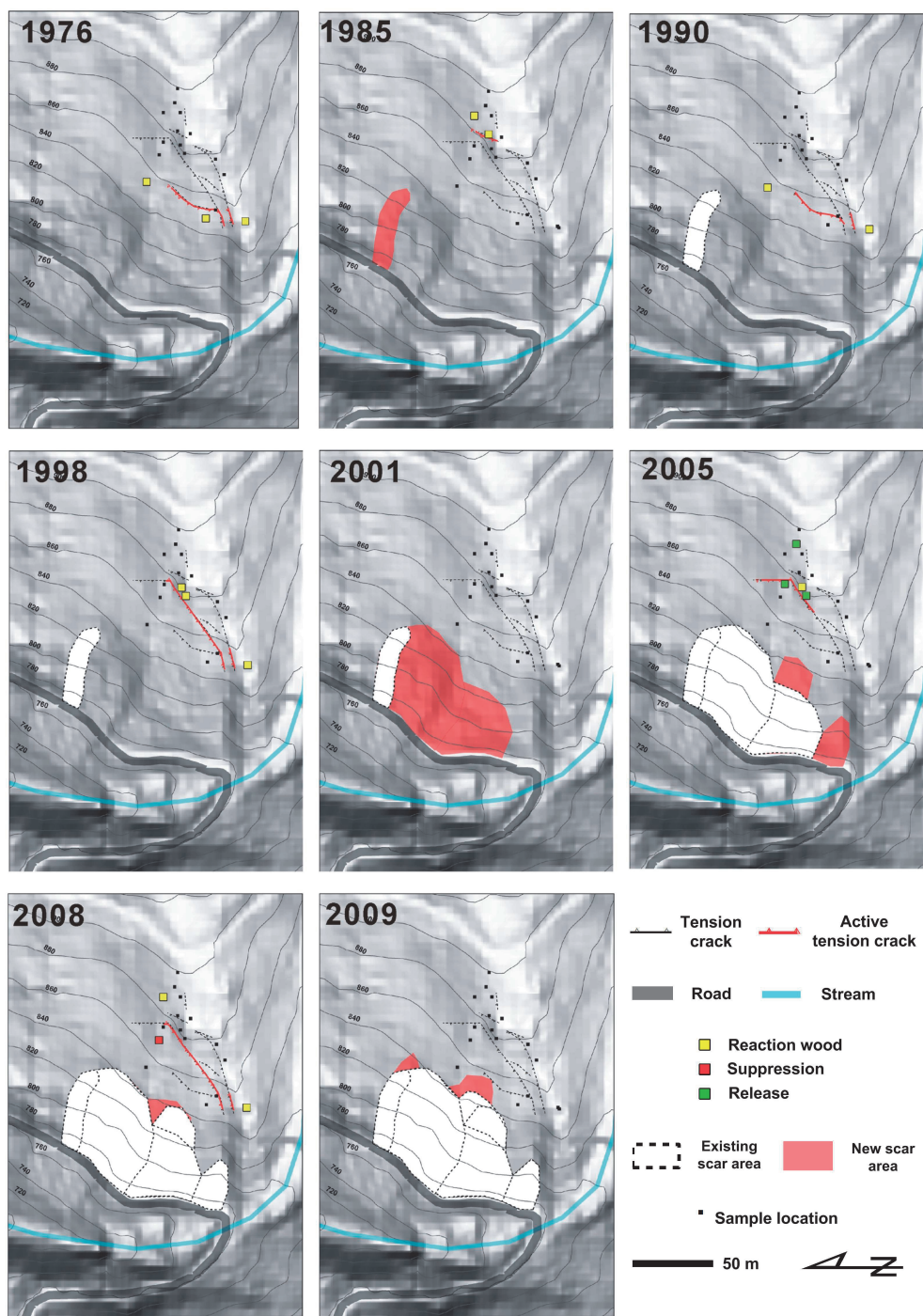

Fig.11　Scar activity and growth disturbance map, contour interval = 20 m

Between 1974 and 2011, over 1,650 events occurred. For each event, event accumulated rain and mean rainfall intensity (mean 1 hr. accumulated rainfall) were calculated. Rainfall characteristics are shown in Fig. 12. In general, estimated years of activity coincide well with years of high annual accumulated rainfall. Years of landslide activity also seem to coincide with many high accumulated rainfall events. Mean rainfall intensity is relatively consistent every year and does not appear to coincide with years of landslide activity.

V. Discussion

1. Activity at the head of the landslide

Two failure patterns can be identified from the landslide activity record: (1) scar activity at the foot of the landslide preceded by activity at the head of the landslide body and (2)scar activity at the foot of the landslide paired with activity at the head of the landslide. Scar activity in 1985 was preceded by activity at the head of the landslide in 1976 and scar activity in 2001 was preceded by two instances of activity at the head that occurred in 1990 and 1998.

An explanation for scar activity preceded by activity at the head of the landslide may be that as the landslide body slowly shifted downslope, such as it might have been doing in 1990 and 1998, displacement was neither rapid or large enough to destabilize the foot of the landslide. By 2001 though, the accumulated displacement of the foot may have been large enough to cause destabilization. However, it should be noted, in the 2001 aerial photo, the road has been recently widened, suggesting that destabilization of the landslide foot could have been caused or accelerated by road construction activities.

Scar activity at the foot of the landslide paired with activity along the features around the head of the landslide body may have been caused by rapid and large displacement of the entire land-

slide body. Recent landslide events in 2005 and 2008 have included activity at both the head and foot of the landslide, which may suggest that downward movement of the landslide body has accelerated in recent years.

2. Landslide activity and rainfall threshold exceedance events

From the 1,650 storm events that occurred between 1974 to 2011, possible landslide-causing storm events were identified using a 5% exceedance probability, intensity-duration(ID) threshold(Brunetti et al., 2010; Taiwan Central Geologic Survey, 2011) for the geologic region with which the landslide occurred(Interbedded sandstone and shale region, Taiwan Central Geologic Survey, 2012). That ID exceedance threshold and all storm events are shown in Fig. 13 A. Any event that did not exceed the ID threshold is marked by a black dot. Any event that exceeded the ID threshold but did not occur during years of estimated landslide activity(non-landslide years) are marked by a white polygon. Storm events that exceeded the ID threshold and occurred during a landslide year are marked by a polygon and shaded according to the ID threshold level exceeded: storms that exceed the 5% ID threshold are shaded grey and storms that exceed the 50% ID threshold are shaded black. Event duration is indicated by the shape of the polygon.

Using only the storm events that exceeded the ID threshold(white and shaded polygons), landslide year and non-landslide year storm events were compared by examining the mean difference of rainfall characteristics listed in Table 1. To investigate the influence of seasonal accumulated rain, seasonal accumulated rain was divided into three types based on the five rainfall regimes in Taiwan(Chen and Chen, 2003). For each seasonal accumulated rain category, accumulated rain is calculated from the beginning of the regime to the hour before the event. The seasons investigated are: Winter(January to Event), Mei-Yu(May to Event), and Summer season(July to Event) accumulated rain.
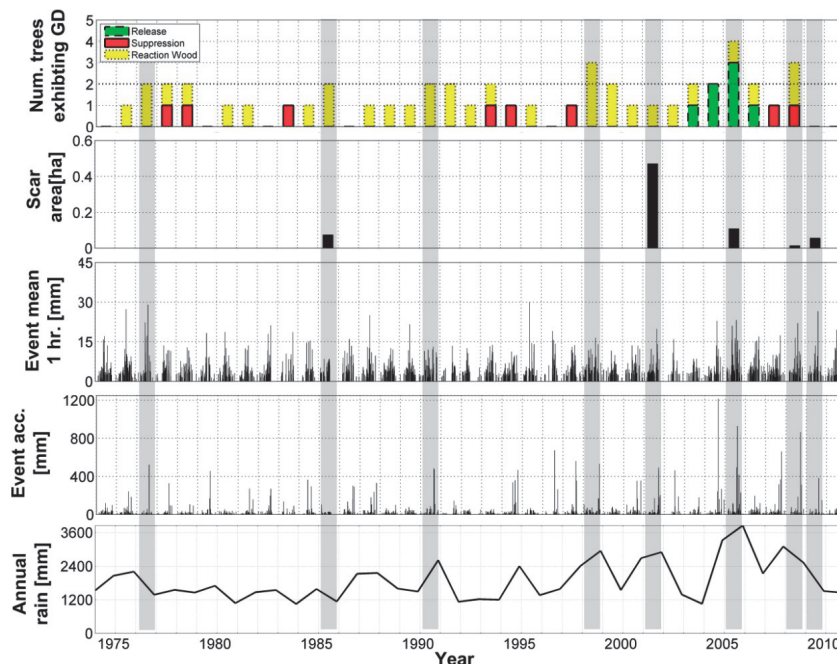

Fig.12 Estimated years of landslide activity and event and annual rainfall conditions between 1974 and 2011

Of the rainfall characteristics investigated, the largest mean differences were found for summer accumulated, event accumulated rain and winter accumulated rain which had means that were 153, 138 and 134 % the non-landslide year mean respectively. Seven day antecedent rainfall was 131 % of non-landslide years while intensity was only 108 % of non-landslide years. Regarding the reliability of the mean difference estimate, only winter accumulated rain had a 95% true mean confidence interval for the true mean difference that did not contain zero and therefore seems to be the most reliable value. The plausible values for summer accumulated rain and event accumulated rain include zero only at the fringe of the interval. The 95% true mean confidence interval for seven day antecedent rainfall and intensity both include zero near the center of the interval, suggesting that the true mean difference may actually be much smaller than the estimated difference.

Rainfall characteristics of the possible landslide-causing storm events are plotted as intensity versus duration, intensity versus event accumulated rain(Jan et al., 2003), event accumulated rain versus 7 day antecedent rain(Yu et al., 2006), and event accumulated rain versus seasonal accumulated rain(Gabet et al., 2004) in Fig. 13 A, B, C and D respectively. In all plots except event accumulated rain versus seasonal rain, events that occurred during landslide years plot intermixed with events that occurred during non-landslide years; no clear trend distinguishes landslide years from non-landslide year storm events.
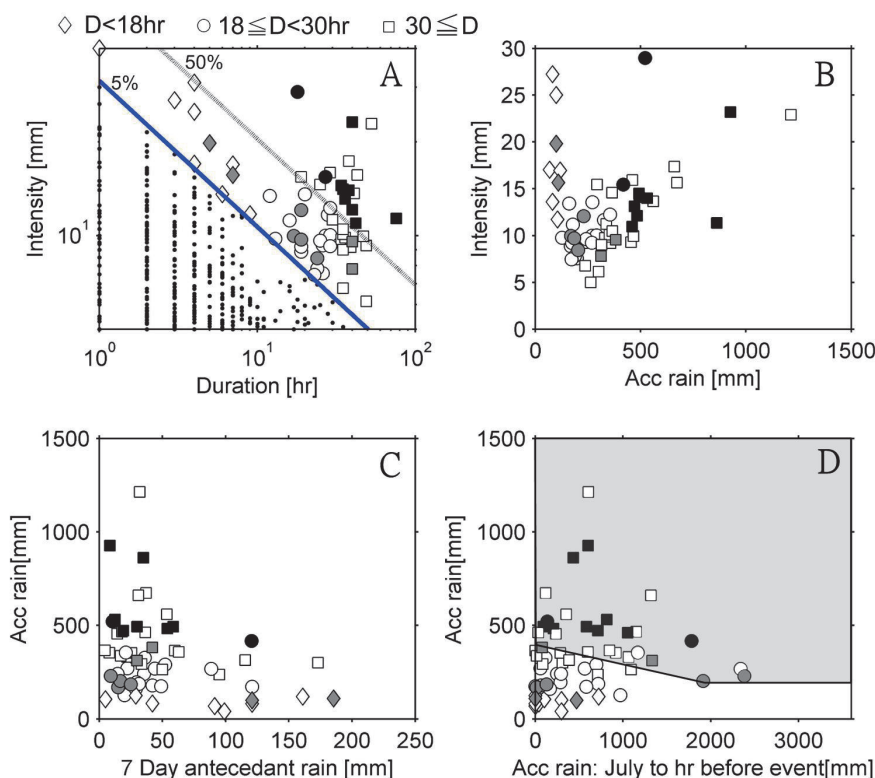
Fig.13 Rainfall characteristics for all events that occurred between 1974 to 2011. In Fig. 13 A, rainfall events less than the 5% Intensity-Duration(ID) threshold(blue line) are marked as small points and events that exceed the 5% ID threshold are marked by a polygon according to event duration(D). If the year the that the event occurred coincides with a year that landslide activity was recorded, the polygon is shaded according to the ID threshold level exceeded: events that exceed the 5% ID threshold are shaded grey and events that exceed the 50% ID threshold are shaded black. Landslide year and non-landslide year events plot intermixed in Fig. 13 B and C. However, in Fig. 13 D, landslide year and non-landslide year events are more distinctly grouped and a rainfall threshold based on event accumulated rain and summer accumulated rain has been identified

Table 1   A comparison of landslide year and non-landslide year rainfall events that exceeded the 5% rainfall threshold

Mean rain characteristic	Landslide years± std	Non-landslide years±std	Mean difference	95% Confidence interval for true mean difference
Jan to Dec, Annual Accumulated [mm]	2360±936	1894±705	466	-114 to1047
Event intensity: mean hourly accumulated [mm]	14±5	13±7	1	-3 to 4
Event Accumulated [mm]	408±231	296±206	112	-7 to 233
Event 7 day antecedent accumulated rain [mm]	72±117	55±51	17	-26 to 60
Winter (Jan) to Event accumulated [mm]	1604±827	1194±567	410	44 to 777
Meiyu (May) to Event accumulated [mm]	1099±767	851±505	248	-85 to 581
Summer(July) to Event accumulated [mm]	708±717	463±486	245	-71 to 560
Event Duration [hr]	31±16	26±14	5	-3.7 to 13

Plotted as event accumulated rain versus seasonal rain and ignoring an isolated group of high intensity, short duration storm events, a clear separation between landslide year and non-landslide year storm events is distinguishable and a rainfall threshold specific to the Tieliku mingsui landslide can be identified(Fig. 13 D). Ignoring the short duration, high intensity storms may be justified since those storms occurred during years that high event accumulated rain events also occurred. Also, the true mean difference between the intensity of events that occurred during landslide years and non-landslide years may be close to zero(Table 1).

The event accumulated and seasonal rainfall threshold indicates that single events having accumulated rainfall exceeding 400 mm may trigger landslide activity regardless of summer accumulated rain. However during years that summer rain has already totaled 1900 mm, events having accumulated rainfall as low as 200 mm may trigger landslide activity. This relationship between event accumulated rain, seasonal rain and landslide occurrence resembles the relationship found for a Himalayan catchment reported in Gabet et al. (2004). Like the landslides occurring in that Himalayan catchment, the Tieliku mingsui landslide is occurring within a thick, fractured bedrock layer. Before the bedrock reaches field capacity, high event accumulated rain or a combination of high seasonal rain and event rain is required.

3. Small, mixed species sample group

Past dendrogeomorphic studies, such as Lopez et al. (2012), used hundreds of pine trees to identify periods of landslide activity for a 32 ha landslide. In other studies, such as Carrara and O'Neil (2003), 32 conifers, sampled from three separate landslides, were used to estimate years of earthquake caused landslide activity. In this study, 17 trees, including both broadleaf and conifers, were sampled from a single 1.5 ha landslide. Accuracy of landslide activity estimates were improved by utilizing a reference chronology. Also, coincident years of both growth disturbance and aerial photo and satellite image derived activity estimates suggest periods of activity were correctly identified. However, study results would have been strengthened by a larger, single species sample group.

VI. Conclusions

Remote sensing observations combined with a VBS-RTK survey of landslide features and a dendrogeomorphic investigation on trees growing near those features reveals the location and timing of 8 landslide events for the Tieliku Mingsui landslide; a deep seated, medium sized landslide occurring in fractured argillite and sandy shale stone bedrock.

Two types of landslide mechanisms have been identified: (1)scar activity at the foot of the landslide preceded by activity at the head of the landslide body and (2)scar activity at the foot of the landslide paired with activity at the head of the landslide.

Rainfall characteristics that may have caused landslide activity have also been identified and used to develop a rainfall threshold for landslide activity. Of the landslide year and non-landslide year rainfall characteristics compared, the mean difference was greatest for summer (July to event) accumulated rain and smallest for intensity. The rainfall threshold, based on event accumulated rain and summer accumulated rain, reveals that event accumulated rainfall exceeding 400 mm may trigger landslide activity regardless of summer accumulated rain. During wetter summers, when summer accumulated rain has exceeded 1900 mm, events having accumulated rainfall as low as 200 mm may trigger landslide activity.

References

[1]   Alestalo, J. (1971). "Dendrochronological interpretation of geomorphic processes." Fennia, 105, 1-139.

[2]   Baker, P.J., Bunyavejchewin, S., Oliver, C.D., and Ashton, P.S. (2005). "Disturbance history and historical stand dynamics of a seasonal tropical forest in western Thailand." Ecological Monographs, 75(3), 317-343.

[3]   Bollati, I., Dell-Seta, M., Pelfini, M., Del-Monte, M., Fredi, P., and Lupia-Palmieri, E. (2007). "Dendrochronological and geomorphological investigations to assess water erosion and mass wasting processes in the Apennines of Southern Tuscany(Italy)." Catena, 90, 1-17.

[4]   Bollschweiler, M., Stoffel, M., Ehmisch, M., and Monbaron, M. (2007). "Reconstructing spatio-temporal patterns of debris-flow activity using dendrogeomorphological methods." Geomorphology, 87, 337-35.

[5]   Borga, M., Fontana, G.D., DaRos, D., and Marchi, L. (1998). "Shallow landslide hazard assessment using a physically based model and digital elevation data." Environmental Geology, 35, (2-3).

[6]   Braam, R.R., Weiss, E.E.J., and Burrough, P.A. (1987). "Spatial and temporal analysis of mass movement using dendrochronology." Catena, 14, 573-584.

[7]   Brunetti, M.T., Peruccacci, S., Rossi, M., Luciani, S., Valigi, D., and Guzzetti, F. (2010). "Rainfall thresholds for the possible occurrence of landslides in Italy." Natural Hazards and Earth System Sciences 10, 447-458.

[8]   Capart, H., Hsu, P., Lai, Y.J., and Hsie, M.S. (2010) "Formation and decay of a tributary dammed lake, Laonong river, Taiwan." Water Resources Research 46.doi:10.1029/2010WR009159

[9]   Carrara, P.E., and O'Neil, J.M. (2003). "Tree-ring dated landslide movements and their relationship to seismic events in southwestern Montana, USA." Quaternary Research, 59, 25-35.

[10] 經濟部中央地質調查所 (2011) 「強化豪雨引致山崩之即時動態潛勢評估與警戒模式」，經濟部中央地質調查所，台灣。(Central Geology Survey (2011). "Development of a real-time rainfall triggered landslide evaluation and warning system." Taiwan Central Geology Survey, Taiwan.(In Chinese))

[11] Central Geological Survey (2012). "Integrated Geological Data Inquiry System. Ministry of Economic Affairs." Tai-

wan. http://www.moeacgs.gov.tw/info/view.jsp?info=462. Accessed June, 2012.

[12] Chang, J., Chung, F., Fabbri, A.G. (1999). "Probabilistic prediction models for landslide hazard mapping." Photogrammetric Engineering & Remote Sensing, 65(12), 1389-1399.

[13] Chen, C.S., and Chen, Y.L. (2003). "The Rainfall Characteristics of Taiwan." American Meteorological Society, 131(7), 1323-1341.

[14] Cook, E.R., and Kairiukstis, L.A. (1990). Methods of Dendrochronology, Applications in the Environmental Sciences. Kluwer Academic Publishers

[15] Cornforth, D.H. (2005). Landslides in Practice: Investigation, analysis and remedial/preventative options in soils. John Wiley & Sons New Jersey, 4-5.

[16] IAEG Commission on landslides, (1990). In Special report 247, Landslides investigation and mitigation, Turner AK, Schuster, RL(eds.) TRB, National Research Council(US), Washington D.C.

[17] Cruden, D.M., and Varnes, D.J. (1996). "Landslide types and processes." In Special report 247, Landslides investigation and mitigation, Turner AK, Schuster, RL(eds.) TRB, National Research Council(US), Washington D.C.

[18] Fantucci, R., and Sorriso-Valvo, M. (1999). "Dendrogeomorphological analysis of a slope near Lago, Calabria(Italy)." Geomorphology, 30(1-2), 165-174.

[19] Fritts, H.C. (1976). Tree Rings and Climate. New York and San Francisco. Academic Press.

[20] 馮豐隆，詹明勳 (2005) 「年輪學應用於森林與環境的關係」，林學研究季刊，27(3)，37-50。(Feng, F.L., and Chan, M.C. (2005). "Application of Dendrochronology in the relationship of forest and environment." Quarterly Journal of Chinese Forestry, 27(3), 37-50. (In Chinese))

[21] Gabet, E.J., Burbank, D.W., Putkonen, J.K., Pratt-Sitaula, B.A., and Ojha, T. (2004). "Rainfall thresholds for landsliding in the Himalayas of Nepal." Geomorphology 63, 131-143.

[22] Grissino-Mayer, H.D.(2001). "Evaluating crossdating accuracy: A manual and tutorial for the computer program COFECHA." Tree-Ring Research, 57(2), 205-221.

[23] Holmes, R.L. (1983). "Computer-assisted quality control in tree-ring dating and measurement." Tree-Ring Bulleting, 43.

[24] Hovius, N., Stark, C.P., Chu, H.T., and Lin, J.C. (2000). "Supply and removal of sediment in a landslide dominated mountain belt: central range, Taiwan." The Journal of Geology ,108(1), 73-89.

[25] 詹錢登、李明熹、黃婷卉 (2003) 土石流發生降雨警威值模式之研究，九十一年度防救災專案計畫成果研討會，8.1-8.20，台北，台灣。(Jan, C.D., Lee, M.H., and Huang, T.H. (2003). "Rainfall Threshold Criterion for Debris Flow Initiation." Annual Meeting on Hazards Mitigation Research, pp.8.1-8.20, Taipei, Taiwan(In Chinese))

[26] Larsen, M.C., and Simon, A. (1993). "A rainfall intensity-duration threshold for landslides in a humid-tropical en-

vironment, Puerto Rico." Geografiska Annaler, 75A(1-2), 13-23.

[27] Lin, W.T., Lin, C.Y., and Chou, W.C. (2006). "Assessment of vegetation recovery and soil erosion at landslides caused by a catastrophic earthquake: A case study in Central Taiwan." Ecological Engineering, 28(1),79-89.

[28] Lopez-Saez, J., Corona, C., Stoffel, M., Astrade, L., Berger, F., and Malet, J.P. (2011). "Dendrogeomorphic reconstruction of past landslide reactivation with seasonal precision: the Bois Noir landslide, southeast French Alps." Landslides 9(2), 189-203.

[29] Lopez-Saez, J., Corona, C., Stoffel, M., Schoenieich, P., and Frederic Berger, F. (2012). "Probability maps of landslide reactivation derived from tree-ring records: Pra Bellon landslide, southern French Alps." Geomorphology, 138,189-202.

[30] Migon, P., Panek, T., Malik, I., Hradecky, J., Owczarek, P., and Silhan, K. (2010) "Complex landslide terrain in the Kamienne Mountains, Middle Sudetes, SW Poland." Geomorphology, 124, 200-214.

[31] Montgomery, D.R., and Dietrich, W.E. (1994). "A physically based model for the topographic control on shallow landsliding." Water Resources Research, 30(4), 1153-1171.

[32] Montgomery, D.R., Schmidt, K.M., Greenberg, H.M., and Dietrich, W.E. (2000). "Forest clearing and regional landsliding." Geology, 28(4), 311-314

[33] Pistocchi, A., Luzi, L., and Paola, N. (2001). "The use of predictive modeling techniques for optimal exploitation of spatial databases: a case study in landslide hazard mapping with expert system-like methods." Environmental Geology, 41(7), 765-775.

[34] Roering, J.J, Kirchner, J.W., and Dietrich, W.E. (2005). "Characterizing structural and lithologic controls on deep-seated landsliding: Implications for topographic relief and landscape evolution in the Oregon Coast Range, USA." GSA Bulletin 117(5-6) doi: 10.1130/B25567.1

[35] Schroder, J.F. (1978). "Dendrogeomorphological analysis of mass movement on table cliffs plateau, Utah." Quaternary Research, 9,168-185.

[36] Speer, J.H. (2010). Fundamentals of Tree-Ring Research, The University of Arizona Press.

[37] Stoffel, M. (2005). "A review of studies dealing with tree rings and rockfall activity: The role of dendrogeomorphology in natural hazard research." Natural Hazards, 39, 51-70.

[38] Stoffel, M., Bollschweiler, M., Butler, D., and Luckman, B. (2010). Tree Rings and Natural Hazards, Springer, New York.

[39] Stokes, M.A., and Smiley, T.L. (1968). An Introduction to Tree Ring Dating, University of Arizona Press.

[40] Tsai, Z.X., You J.Y., Lee H.Y., and Chiu Y.J. (2011), "Use of a total station to monitor post-failure sediment yields in landslide sites of the Shihmen reservoir watershed, Taiwan," Geomorphology, 139-140, 438-451.

[41] Tsou, C.Y., Feng, Z.Y., and Chigira, M. (2011). "Catastrophic landslide induced by Typhoon Morakot, Shiaolin, Taiwan." *Geomorphology,* 127, 166-178.

[42] Wen, H.Y., Hsu, S.M., and Chiou, L.B. (2012). "Watershed sediment yield estimate with sources of point and non-point sediment during heavy rain period." *Journal of the Chinese Institute of Civil and Hydraulic Engineering,* 24(1), 85-99.

[43] Wang, W.N., Wu, H.L., Nakamua, H., Wu, S.C., Ouyang, S., and Yu, M.F. (2003). "Mass movements caused by recent tectonic activity: The 1999 Chi-chi earthquake in central Taiwan." The island Arc, 12,325-334.

[44] Wang, X.C., and Zhao, Y.F. (2011). "Growth release determination and interpretation of Korean pine and Koyama spruce in Shengshan National Nature Reserve, Heilongjiang Province, China." Acta Ecologica Sinica 2011,31(5), 1230-1239.

[45] 王松永、丁昭義 (1979)，「林產學 上冊」，臺灣商務印書館，台灣，647-655。(Wang, S.Y., and Ding, Z.Y. (1979). Forest Products, The Commercial Press, Ltd., Taiwan, 647-655. (In Chinese))

[46] Yu, F.C., Chen, T.C., Lin, M.L., Chen, C.Y., and Yu, W.H. (2006). "Landslides and rainfall characteristics analysis in Taipei City during the typhoon Nari event." Natural Hazards 37(1-2), 153-167.